PHYSICAL REVIEW B **96**, 134405 (2017)

Magnetic and structural properties of $FeCO_3$ at high pressures

N. O. Golosova,[1] D. P. Kozlenko,[1] L. S. Dubrovinsky,[2] V. Cerantola,[3] M. Bykov,[2] E. Bykova,[2,4] S. E. Kichanov,[1] E. V. Lukin,[1]
B. N. Savenko,[1] A. V. Ponomareva,[5] and I. A. Abrikosov[6]
[1]*Frank Laboratory of Neutron Physics, Joint Institute for Nuclear Research, 141980 Dubna, Russia*
[2]*Bayerisches Geoinstitut, Universität Bayreuth, D-95440 Bayreuth, Germany*
[3]*European Synchrotron Radiation Facility, BP 220, F-38043 Grenoble, France*
[4]*Photon Sciences, Deutsches Elektronen Synchrotron, D-22607 Hamburg, Germany*
[5]*Materials Modeling and Development Laboratory, National University of Science and Technology "MISIS", 119049, Moscow, Russia*
[6]*Department of Physics, Chemistry and Biology (IFM), Linköping University, SE-58183 Linköping, Sweden*
(Received 14 June 2017; revised manuscript received 11 September 2017; published 3 October 2017)

The structural and magnetic properties of siderite $FeCO_3$ have been studied by means of neutron powder diffraction at pressures up to 7.5 GPa and first-principles theoretical calculations. The lattice compression in the rhombohedral calcite-type structure is dominated by the reduction of the Fe-O bonds, while the changes of the C-O bonds are much less pronounced. The Néel temperature of the antiferromagnetic (AFM) ground state increases substantially under pressure with a coefficient $dT_N/dP = 1.8\,\mathrm{K/GPa}$, which is about 1.5 times larger in comparison with those predicted by the empirical Bloch rule. The *ab initio* calculations were performed in the framework of the density functional theory including Hubbard-U correction. The calculated structural parameters and Néel temperature as functions of pressure provide a reasonable agreement with the experimental results. The analysis of the density of electronic states points toward increased covalent bonding between the Fe and O atoms upon pressure, giving rise to unexpectedly large pressure coefficient of the Néel temperature and reduced ordered magnetic moments of Fe atoms.

DOI: 10.1103/PhysRevB.96.134405

I. INTRODUCTION

The iron carbonate $FeCO_3$ (siderite mineral) is a simple material, with a structural arrangement that provides nearly perfect realization of the three-dimensional magnetic Ising system in crystals [1,2]. The electromagnetically induced transparency phenomenon via unusual nuclear-level anticrossing scheme discovered in siderite for gamma rays makes it prospective for applications in the field of nuclear quantum optics [3,4]. In addition, iron bearing carbonates are considered to play an important role in the deep carbon cycle of the Earth, attracting significant interest to studies of physical properties of such compounds under variation of thermodynamics parameters [5,6].

The siderite $FeCO_3$ crystallizes in the rhombohedral calcite-type structure of $R\bar{3}c$ symmetry, formed by corner-shared trigonal planar CO_3 groups and FeO_6 octahedra [7]. The long-range antiferromagnetic (AFM) order occurs below the Néel temperature $T_N \approx 38\,\mathrm{K}$ [8,9]. The ordered magnetic moments of Fe^{2+} ions are arranged in the ferromagnetic (FM) layers perpendicular to the c axis (in hexagonal setting) with antiferromagnetic coupling between the neighboring layers. The paramagnetic-antiferromagnetic phase transition in $FeCO_3$ serves as a model example for testing predictions of the three-dimensional magnetic Ising system [1,2,10].

Recently, a pressure-induced phase transition was observed in siderite at $P \sim 40-50\,\mathrm{GPa}$, associated with the spin-state crossover of Fe^{2+} ions from the high-spin (HS, $S = 2$) to the low-spin (LS, $S = 0$) state [11–14]. The transition is accompanied by the volume collapse and the shrinkage of the bonds forming FeO_6 octahedral units [13]. The modifications of the crystal structure and electronic configuration of Fe^{2+} ions in $FeCO_3$ were previously studied in detail using x-ray diffraction and various spectroscopy techniques in the extended pressure range [11–14]. However, a response of the long-range magnetic order upon lattice compression remains poorly explored. Its clarification is important for general understanding of the structure-properties relationship of the three-dimensional Ising model systems as well as microscopic mechanisms of the spin-state crossover in siderite. In this paper, we studied high-pressure effects on the crystal and magnetic structure of siderite by means of neutron powder diffraction at high pressures up to 7.5 GPa. *Ab initio* theoretical calculations were performed for the interpretation of the experimental data.

II. EXPERIMENTAL AND COMPUTATIONAL DETAILS

A synthetic siderite was used as the object of this study. Natural siderite powder was considered undesirable because of the common partial oxidation of the material and the amounts of other divalent cations generally present in solid solution, the most common Mg^{2+}, Mn^{2+}, and Co^{2+}. Siderite used in this study was synthesized by decomposition of ferrous oxalate dehydrate $FeC_2O_4 \cdot 2H_2O$. Its powder was sealed in gold capsules of 2.3 mm outer diameter, loaded into an externally heated cold seal vessel, and stored at 2 kbars and 360 °C for 7 days, following the procedure described by French [15]. The obtained siderite was characterized by the x-ray powder diffraction, Mössbauer and Raman spectroscopy, and it did not show any trace of Fe-oxides or other impurities (see also Cerantola *et al.*) [14].

Neutron powder diffraction measurements at high pressures up to 7.5 GPa were performed at selected temperatures in the range 10–290 K with the DN-6 diffractometer at the IBR-2 high-flux pulsed reactor (FLNP JINR, Dubna, Russia). The sample with a volume of about $2\,\mathrm{mm}^3$ was loaded into the sapphire anvil high pressure cell without additional pressure

2469-9950/2017/96(13)/134405(7)

©2017 American Physical Society

medium [16]. The anvils with the culets of 2 mm were used and the spherical holes of the 1-mm diameter were drilled in the culet centers to attain quasihydrostatic pressure distribution on the sample surface. Several tiny ruby chips were placed at different points of the sample surface and the pressure was determined by a standard ruby fluorescence technique. Measurements of the pressure distribution on the sample yield typical pressure inhomogeneities of ±15%. Diffraction patterns were collected at scattering angle 90° with the resolution $\Delta d/d = 0.012$. Experimental data were analyzed by the Rietveld method using the Fullprof program [17].

The *ab initio* calculations were performed using the supercell technique and all electron projector-augmented-wave (PAW) method [18], as implemented in the VASP code [19,20]. The simulations were carried out using the $2 \times 2 \times 2$ 80-atoms periodic supercells. A sampling of the Brillouin zone was done using a Monkhorst-Pack scheme [21] on a grid of $10 \times 10 \times 10$ k-points. Gaussian smearing method was chosen with a smearing width of 0.05 eV. The electronic density of states was calculated by the tetrahedron method with Blöchl corrections [22]. The energy cutoff for the plane waves included in the expansion of wave functions was set to 500 eV. The convergence criterion for the electronic subsystem was chosen to be equal to 10^{-4} eV for two subsequent iterations, and the ionic relaxation loop within the conjugated gradient method was stopped when forces became of the order of 10^{-3} eV/Å. The local magnetic moments at Fe atoms were obtained by integrating the magnetization density within the corresponding Wigner-Seitz sphere. The magnetic moment of Fe^{2+} ions calculated in this way at $P = 0$ GPa was $\sim 3.7\,\mu_\mathrm{B}$, which corresponded to $3d^6$ electronic configuration. Moreover, we found that the charge associated with Fe site calculated directly by VASP ($q = 6.61e$) was very close to the value obtained from the Bader analysis ($q_\mathrm{B} = 6.56e$).

To calculate the magnetic ordering energy needed for an estimation of the pressure dependence of the Néel temperature, it was necessary to determine the energy of the paramagnetic state of $\mathrm{FeCO_3}$. The latter was described within the disordered local moments (DLM) model [23,24]. The calculations were carried out using the magnetic special quasirandom structure technique (MSQS) [25]. The generated MSQS for modeling of the DLM of a state represented two types of magnetic structure–with spin flips at 1 or 2 Fe atoms in a four-atoms layers perpendicular to the c axis. The results for both MCQS are close to each other, so here we give only the result for the first. The difference of the DLM and AFM total energies per magnetic atom in the system, which is the magnetic ordering energy ΔE_magn, in the classical Heisenberg model directly provides the approximate value of the nearest-neighbor pair exchange parameter J_0:

$$J_0 = \Delta E_\mathrm{magn} = (E^\mathrm{DLM} - E^\mathrm{AFM}).$$

A qualitative estimate of the pressure variation of the Néel temperature was carried out in the mean-field approximation [26]:

$$k_B\, T_N = \frac{2}{3}\sum_j J_{0j} = \frac{2}{3}\, J_0,$$

where $J_{0\mathrm{j}}$ is the nearest-neighbor pair exchange parameter of the classical Heisenberg Hamiltonian $H = -\sum J_{\mathrm{ij}} e_i e_j$, e_i is a unit vector specifying the direction of the magnetic moment on the ith site.

The exchange and correlation effects have been approximated using the generalized gradient approximation [27] (GGA) augmented by including Hubbard-U corrections within the framework of the density functional theory (the DFT + U method), following the Dudarev's approach [28]. We have chosen parameters $U = 4$ eV and $J = 1$ eV for the Fe d states, provided the value of t_{2g}-e_g energy splitting about 1.1 eV, in a good agreement with the data reported by Lobanov *et al.* [29]. Indeed, these authors observed a weak and wide absorption band at ambient pressure with the center in the region of $10\,325\ \mathrm{cm}^{-1}$ (1.28 eV), which they assigned to electronic transition $5t_{2g} \rightarrow 5e_g$.

III. RESULTS AND DISCUSSION

A. Neutron diffraction

Neutron diffraction patterns of $\mathrm{FeCO_3}$ measured at selected pressures and temperatures with the DN-6 diffractometer and analyzed by the Rietveld method are shown in Fig. 1. The

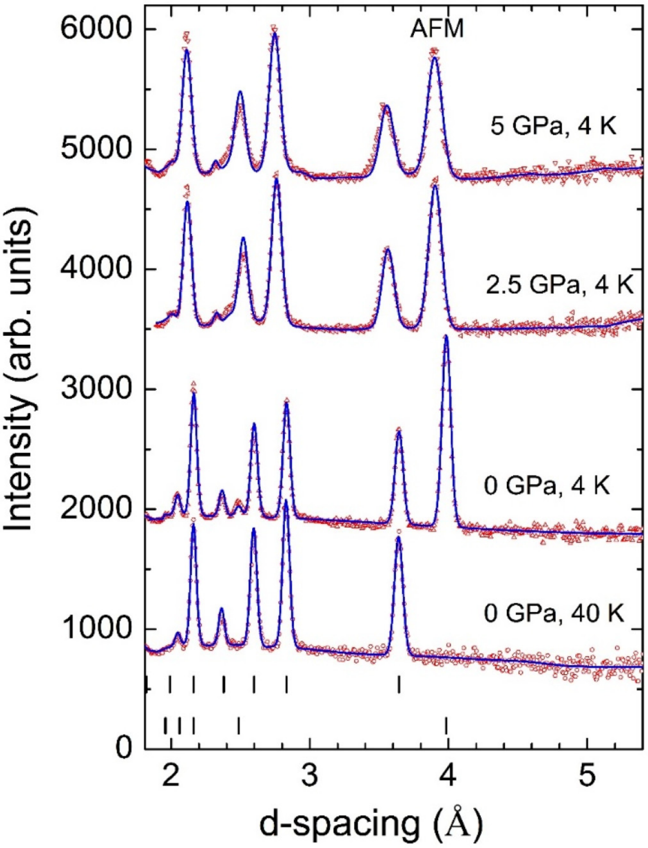

FIG. 1. Neutron diffraction patterns of $\mathrm{FeCO_3}$, measured at $P =$ 0, 2.5, and 5 GPa, $T = 4$ and 40 K and processed by the Rietveld method. The experimental points and calculated profiles are shown. The ticks below represent positions of structural (upper row) and magnetic (lower row) reflections. The most intense magnetic peak is marked as "AFM".

TABLE I. The obtained structural parameters and ordered Fe magnetic moment values of $FeCO_3$ at selected pressures and temperature $T = 4$ K. The atomic positions are: Fe, 6(b) (0,0,0); C, 6(a) (0,0,0.25); O, 18(e) (x,0,0.25) of the space group $R\bar{3}c$ (in hexagonal setting).

P (GPa)	0	2.5	5.0	7.5
a (Å)	4.7008(17)	4.6647(25)	4.6628(32)	4.6475(39)
c (Å)	15.4036(87)	15.121(13)	14.980(15)	14.822(19)
O: x	0.2648(20)	0.2657(20)	0.2662(20)	0.2660(3)
μ_{Fe} (μ_B)	3.61(5)	3.37(7)	3.38(7)	3.35(9)
Fe-O (Å)	2.170(4)	2.144(5)	2.135(5)	2.123(7)
C-O (Å)	1.245(4)	1.239(5)	1.241(5)	1.236(1)
R_p (%)	5.57	8.52	9.82	7.77
R_{wp} (%)	7.69	11.5	12.8	10.4

siderite rhombohedral structure of $R\bar{3}c$ symmetry remains stable in the investigated pressure range 0–7.5 GPa, in accordance with previous studies [13,14]. The structural parameters obtained from the Rietveld refinement of diffraction data at selected pressures and temperature $T = 4$ K are listed in Table I.

The pressure dependencies of the unit-cell volume and lattice parameters for $FeCO_3$ at $T = 4$ K are shown in Fig. 2. The compressibility data were fitted by the Birch-Murnaghan equation of state [30]:

$$P = \tfrac{3}{2}B_0\left(x^{-\frac{7}{3}} - x^{-\frac{5}{3}}\right)\left[1 + \tfrac{3}{4}(B' - 4)\left(x^{-\frac{2}{3}} - 1\right)\right],$$

where $x = V/V_0$ is the relative volume change, V_0 is the unit cell volume at $P = 0$ GPa, and B_0, B' are the bulk modulus [$B_0 = -V(dP/dV)_T$] and its pressure derivative [$B' = (dB_0/dP)_T$]. The fitted unit cell volume is $V_0 = 293.6(1)$ Å^3. The calculated values $B_0 = 113(5)$ GPa and $B' = 4.0(3)$ are in good agreement with ones $B_0 = 110$ GPa and $B' = 4.6$ found in the x-ray diffraction study at ambient temperature [14]. The obtained bulk modulus B_0 of $FeCO_3$ is comparable with those found for other rhombohedral carbonates like magnesite $MgCO_3$ and rhodochrosite $MnCO_3$, for both of which $B_0 = 107$ GPa [31]. The lattice compression of $FeCO_3$ is strongly anisotropic (Fig. 2). The average compressibility ($k_{ai} = -(1/a_{i0})(da_i/dP)|_T, a_i = a,c$) of the c parameter, $k_c = 0.00181$ GPa^{-1}, is about 3.5 times larger in comparison with that of the a parameter, $k_a = 0.00051$ GPa^{-1}. The anisotropic lattice compression was also found for isostructural carbonates [31].

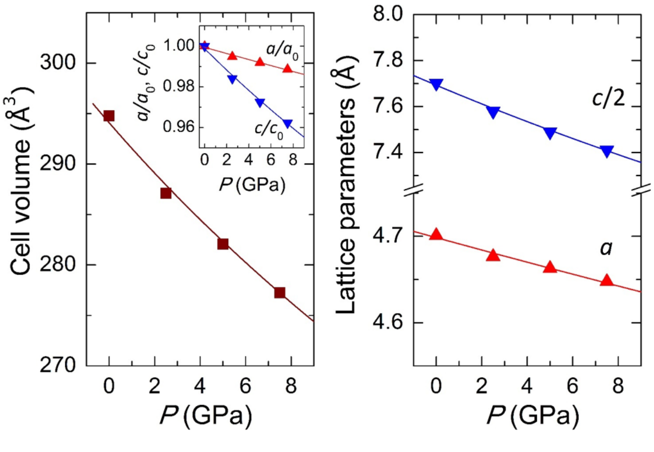

FIG. 2. Unit cell volume and lattice parameters of $FeCO_3$ as functions of pressure obtained at $T = 4$ K and their interpolation based on the Birch-Murnaghan equation of state. Inset: the relative lattice parameters a/a_0 and c/c_0 as functions of pressure.

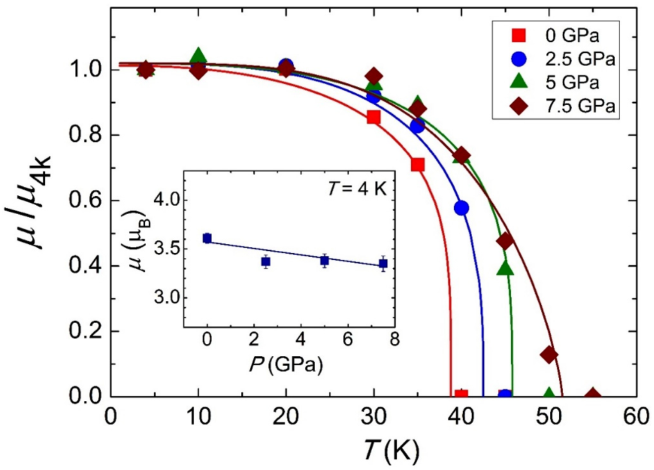

FIG. 3. Temperature dependencies of the ordered Fe magnetic moments of $FeCO_3$ at different pressures normalized to the moment values at $T = 4$ K and their interpolation by functions $\mu = \mu_0(1 - (T/T_N)^\alpha)^\beta$. Inset: pressure dependence of the ordered Fe magnetic moment value at $T = 4$ K and its linear interpolation.

The application of high pressure leads to more significant reduction of the Fe-O bonds (Table I) composing FeO_6 octahedra with the average compressibility $k_{\text{Fe-O}} = 0.0029$ GPa^{-1}. The contraction of C-O bonds forming CO_3 groups is much less pronounced; the relevant average compressibility coefficient is $k_{\text{C-O}} = 0.0009$ GPa^{-1}. The preferential compression of Fe-O bonds over C-O ones was also revealed in single crystal x-ray diffraction study [13].

At ambient pressure upon cooling below the Néel temperature $T_N \approx 38$ K an appearance of magnetic peaks (101)/(−111) at $d \approx 3.95$ Å and (105)/(−115) at $d \approx 2.46$ Å was detected, indicating a formation of the long-range antiferromagnetic order of the Fe^{2+} spins with a propagation vector $q = (0\,0\,1)$ (Fig. 1). The obtained value of the ordered Fe magnetic moment at $T = 4$ K, $\mu_{\mathrm{Fe}} = 3.61\,\mu_B$ (Table I), is comparable with the spin only value expected for the Fe^{2+} ion in the HS state, 4.0 μ_B.

The Néel temperature of $FeCO_3$, calculated from the temperature dependencies of the ordered Fe magnetic moments (Fig. 3), increases from 38 to 52 K in the pressure range 0–7.5 GPa. The corresponding pressure coefficient value is $dT_N/dP = 1.8$ K/GPa. The ordered Fe magnetic moment value at $T = 4$ K exhibits a noticeable reduction from 3.60 to 3.35 μ_B with the pressure increase up to 7.5 GPa (Fig. 3).

In the magnetic ground state of $FeCO_3$ each Fe^{2+} ion is surrounded by six Fe^{2+} neighbors with antiparallel spin alignment and the dominant magnetic interaction is the Fe^{2+}-O^{2-}-Fe^{2+} AFM superexchange. The structural parameters controlling the magnetic interactions strength are Fe-

TABLE II. The calculated structural parameters (lattice constants, oxygen fractional coordinate x, carbon-oxygen (C-O) and the iron-oxygen (Fe-O) bond lengths and magnetic moment of Fe atom μ_{Fe} of $FeCO_3$ in AFM and PM structures at selected pressures. The PM state is simulated within the DLM model.

AFM, 2 × 2 × 2					
P (GPa)	0.6	2.2	4.1	6.8	9.8
a (Å)	4.724	4.720	4.699	4.682	4.662
c (Å)	15.458	15.356	15.198	15.016	14.816
O: x	0.2740	0.2760	0.2766	0.2772	0.2776
μ_{Fe} (μ_B)	3.715	3.714	3.707	3.701	3.700
Fe-O (Å)	2.164	2.145	2.138	2.122	2.090
C-O (Å)	1.297	1.296	1.295	1.293	1.292
DLM, 2 × 2 × 2					
P (GPa)	0.7	2.2	4.1	6.8	9.8
a (Å)	4.7296	4.716	4.700	4.680	4.662
c (Å)	15.481	15.348	15.204	15.012	14.816
O: x	0.2748	0.2762	0.2766	0.2770	0.2773
μ_{Fe} (μ_B)	3.714	3.714	3.706	3.700	3.699
Fe-O (Å)	2.156	2.146	2.138	2.124	2.096
C-O (Å)	1.297	1.296	1.295	1.293	1.292

O-Fe bond angle and Fe-O bond distance. The value of the Fe-O-Fe bond angle is about 118.8(1)° at ambient pressure and $T = 4$ K. It corresponds to relatively weak interaction strength according to the Goodenough-Kanamori-Anderson rules [32]. Upon compression the Fe-O-Fe bond angle remains nearly unchanged and its value is about 118.4° at $P = 7.5$ GPa. This implies that observed increase of the Néel temperature is mainly controlled by a reduction of the Fe-O bond length. The generalized relationship between the lattice compression and modification of the magnetic ordering temperature for antiferromagnetic insulators was formulated in the form of the empirical Bloch rule, $d\log(T_N)/d\log(V) = \alpha = (-10/3) \approx -3.3$ [33]. The calculated value for $FeCO_3$, $\alpha = -5.3$, is about 50% larger in comparison with the expected value.

B. *Ab initio* calculations

The structural parameters of the AFM and paramagnetic (PM) states of siderite and magnetic moments of Fe^{2+} ions calculated in the pressure range 0–10 GPa are presented in Table II. Comparing these theoretical results with experimental data in the Table I, one sees that theoretical calculations accurately reproduce the experimentally observed pressure behavior of the unit cell volume, Fe-O and C-O bond lengths. They are also in consistence with other available experimental [11,13,34,35] and theoretical data [12,36–38].

The CO_3 group is found to be almost incompressible in siderite, while the Fe-O distance decreases with increasing pressure. The calculated Bader charge [39] on Fe (∼6.5e) at $P = 0$ GPa confirms the experimentally determined $3d^6$ configuration of the HS state of the Fe^{2+} ion. At the same time the calculated Fe magnetic moment is ∼3.7 μ_B, which is comparable with the value of $3d^6$ electronic configuration 4 μ_B. The appearance of magnetic disorder (DLM) (Table II) in the PM state practically does not change the structural characteristics of the material over the entire pressure range investigated in this work. The calculated Fe magnetic moments in both structures decrease slightly (∼1%) with increasing pressure up to 10 GPa.

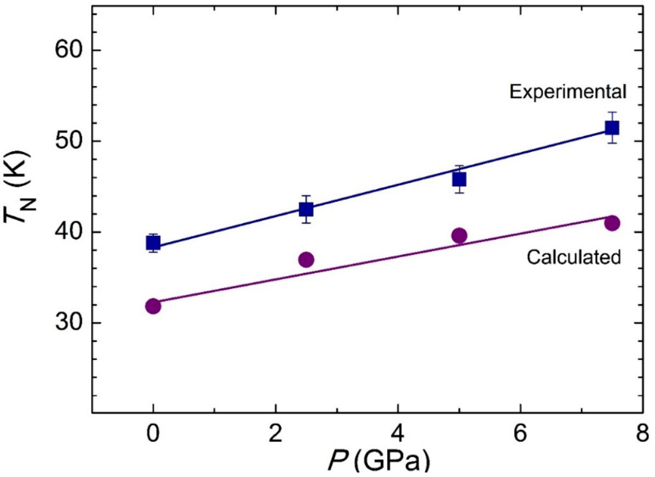

FIG. 4. The experimental and calculated T_N values as functions of pressure.

In agreement with the experiment, the ground state of siderite is found to be antiferromagnetic in the pressure range considered in this study. Indeed, the ferromagnetic state is higher in energy than AFM for all values of the investigated pressures. The pressure behavior of the Néel temperature evaluated in the mean-field approximation is in quite good qualitative agreement with the experimental data, while some systematic difference between the absolute values is present (Fig. 4). The calculated pressure coefficient $(dT_N/dP)_c \approx 1.5$ K/GPa is comparable with the experimental value of 1.8 K/GPa.

To give further insight into the behavior of the AFM and PM states of siderite upon compression, the total and atom-projected density of electronic states (DOS) at pressures $P = 0$ and 10 GPa were calculated (Fig. 5). In both magnetic states, low-energy bands denoted as 6 and 7, are formed by the s electrons of oxygen and carbon. Bands 4 and 5 are formed mainly by p electrons of the O and C atoms. There are strong covalent bonds between the C and O atoms, that is well demonstrated by the calculated electron-localization function (ELF) [40] shown in Fig. 6. The attractor associated with the C-O bond is located half way between the atomic spheres (Fig. 6). Bands 2 and 3 in Fig. 5 consist of the p-O and d-Fe electrons with strong mixing of oxygen and iron states. Density of states in the band 1 comes from localized Fe d states. The bond between the Fe and O atoms is predominantly ionic with the addition of a covalent component. Thus, the siderite $FeCO_3$ exhibits a mixed ionic-covalent chemical bonding.

The main difference in the DOS between the AFM and PM states is a presence of a narrow pseudogap in the former between bands 2 and 3 (Fig. 5). This pseudogap in the AFM state indicates a redistribution of the electronic states with the formation of an almost localized band of p-d hybridized states of Fe and O (band 2). The hybridized orbitals are also formed in the band 3. The appearance of the magnetic disorder in the PM state leads to electron delocalization and a smearing of the boundary between the bands 2 and 3. In the magnetically

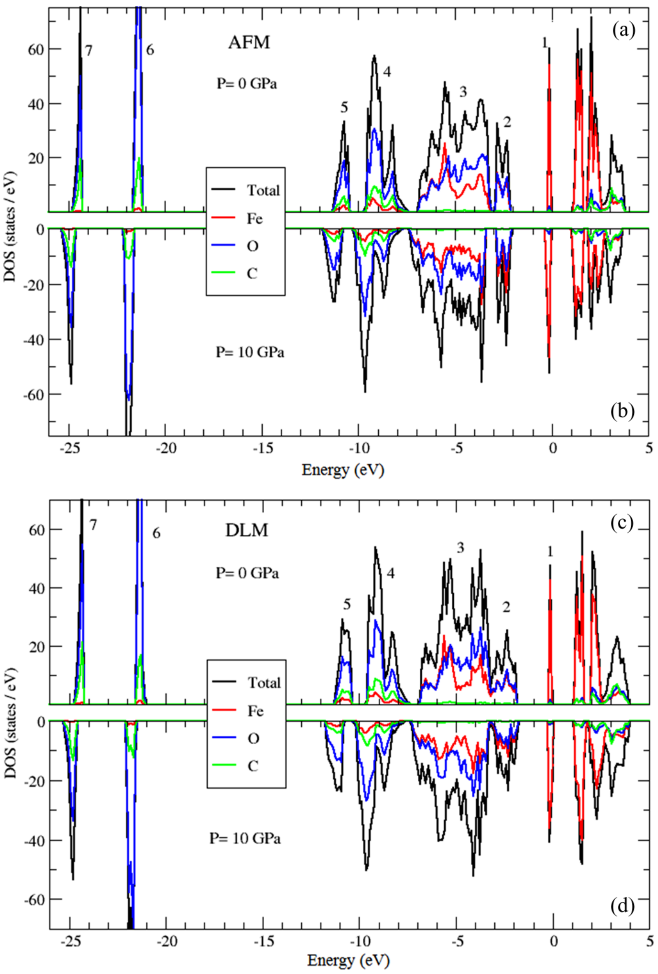

FIG. 5. Calculated density of states (DOS) at $P = 0\,\mathrm{GPa}$ and 10 GPa in AFM (a), (b) and PM (c), (d) states. The PM state is simulated within the DLM model.

ordered AFM state due to the localization of the electronic states the covalent bond between the Fe and O atoms is stronger than in the PM state. The analysis shows that the density of electronic states in the bands 2 and 3 of the AFM state is higher than on the same energy interval in PM state, while the fraction of the electronic states of oxygen and iron in the band 2 is almost identical with the exact coincidence of the peaks.

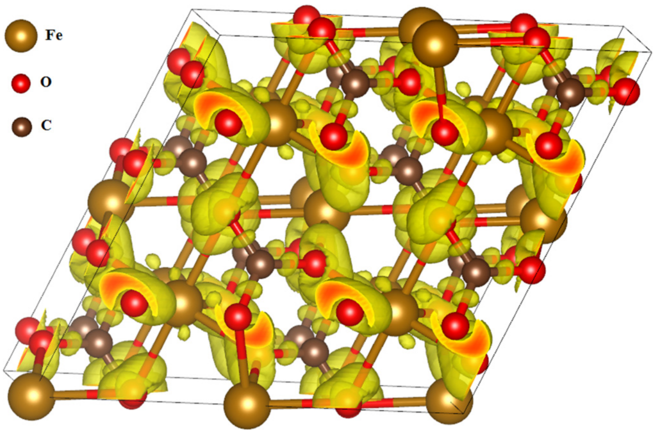

FIG. 6. ELF isosurfaces with ELF = 0.7 in $FeCO_3$ in AFM states at $P = 0\,\mathrm{GPa}$.

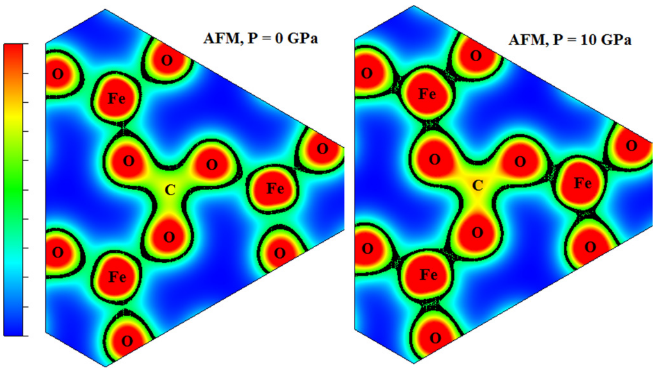

FIG. 7. The charge density maps for Fe-C-O (111) plane in $FeCO_3$ in AFM states at $P = 0\,\mathrm{GPa}$ and 10 GPa.

Upon an increase of pressure up to $\sim 10\,\mathrm{GPa}$, the influence of the crystal field becomes more pronounced. The latter dominates the kinetic energy, and therefore the repulsion between the bands 2 and 3 increases, as well as the pseudogap between them. In this case, a splitting of the bands with the charge redistribution is observed: a sharp narrow peak appears in the region with a high electron density of oxygen [at the upper edge of the band 3, Fig. 5(b)]. The density of states at Fe in the split band 2 also increases. This is accompanied by reinforcement in the covalent bonding due to the strengthening of hybridization of the d orbitals of Fe and p orbitals of O, which leads to the enhancement of the exchange interaction and explains the increased stability of the AFM state upon compression. In the PM state the reinforcement of the covalent bonding with increasing pressure is also observed; however, this process goes significantly slower: at $P = 10\,\mathrm{GPa}$ the deep pseudogap only begins to form.

Summarizing the discussion above, we point out that the distance between the nearest Fe atoms in siderite is too large for a direct exchange interaction. It is realized by overlapping of the wave functions of the $3d$ orbitals of the magnetic Fe ions and p orbitals of nonmagnetic O ions (Fe-O-Fe superexchange). The enhancement of Fe-O hybridization observed in our theoretical analysis of the bond formation mechanism is sufficient to increase the stability of the magnetic order and leads to an unusually high pressure-induced enhancement of the Néel temperature.

To visualize the discussed effect, a map of the charge density in the (111) plane along the Fe-O and C-O bonds in the AFM structure for $P = 0$ and 10 GPa is presented in Fig. 7. It shows that O and C atoms join by common contour lines and form a molecular structural unit linked by strong covalent bonds. In the regions around the Fe^{2+} ions a low charge density is observed. However, despite the predominantly ionic bond between Fe and O atoms the covalent contribution is also seen (left panel, $P = 0\,\mathrm{GPa}$). Most importantly, it increases with pressure, which is confirmed by a compaction of the contour lines on the charge density map (right panel, $P = 10\,\mathrm{GPa}$). In addition, at $P = 10\,\mathrm{GPa}$ the contours of the distribution of charge density around Fe ions display considerable anisotropy.

This is an additional manifestation of strengthening of the covalent contribution to the bonding.

Thus, we demonstrate that reinforcement of the covalent bonding strengthens hybridization between the $3d$ (Fe) and $2p$ (O) orbitals in the AFM state of the siderite upon compression and provides a physically transparent picture of the unexpectedly large pressure coefficient of the Néel temperature and relevant enhancement of superexchange interactions in comparison with that is predicted by the empirical Bloch rule. This effect also explains the observed decrease of the ordered magnetic moments of Fe^{2+} ions in siderite at high pressure. The latter can be tuned by the electron delocalization due to growing covalent component of the bonds between the Fe and O atoms. One should also note that the observed increase of the Néel temperature provides a possible route for the extension of the temperature range for use of the siderite in nuclear quantum optics applications via chemical substitution effects leading to similar structural modification as high-pressure application.

IV. CONCLUSIONS

The present results demonstrate that application of high pressure leads to anisotropic lattice compression of siderite with a major contribution from the Fe-O bonds, while C-O ones are changed only slightly. The antiferromagnetic ground state of siderite remains stable upon compression. The pressure coefficient of the Néel temperature exceeds substantially one predicted by the empirical Bloch rule and the Fe-ordered magnetic moments decrease under pressure.

The *ab initio* calculations performed in the framework of the density functional theory including Hubbard-U correction provide explanation of the experimental results. The analysis of the density of electronic states points towards the increased covalent bonding between the Fe and O atoms upon pressure. The enhanced covalent bonding due to the strengthening of hybridization of the d orbitals of Fe and p orbitals of O atoms is also revealed by theoretical analysis of the charge density variation with pressure. This effect increases the strength of the magnetic superexchange Fe-O-Fe interactions, and it is responsible for the large positive value of the pressure coefficient of the Néel temperature as well as for the reduction of the Fe magnetic moments under pressure.

ACKNOWLEDGMENTS

This work was supported by the Ministry of Education and Science of the Russian Federation (Grant No. 14.Y26.31.0005). I.A.A. is grateful to the support provided by the Swedish Research Council (Grant No. 2015—04391) and the Swedish Government Strategic Research Area in Materials Science on Functional Materials at Linköping University (Faculty Grant SFO-Mat-LiU No. 2009 00971).

[1] J. Kanamori, Prog. Theor. Phys. **20**, 890 (1958).

[2] S. J. Payne, M. E. Hagen, and M. J. Harris, J. Phys.: Condens. Matter **8**, 91 (1996).

[3] R. Coussement, Y. Rostovtsev, J. Odeurs, G. Neyens, H. Muramatsu, S. Gheysen, R. Callens, K. Vyvey, G. Kozyreff, P. Mandel, R. Shakhmuratov, and O. Kocharovskaya, Phys. Rev. Lett. **89**, 107601 (2002).

[4] S. Gheysen and J. Odeurs, J. Phys.: Condens. Matter **20**, 485214 (2008).

[5] R. M. Hazen and C. M. Schiffries, Rev. Mineral. Geochem. **75**, 1 (2013).

[6] M. Isshiki, T. Irifune, K. Hirose, S. Ono, Y. Ohishi, T. Watanuki, E. Nishibori, M. Takata, and M. Sakata, Nature **427**, 60 (2004).

[7] W. G. Wyckoff, *Crystal Structure* (Interscience, New York, 1948).

[8] R. A. Alikhanov, Sov. Phys. JETP **36**, 1690 (1959).

[9] R. F. Altman, S. Spooner, and D. P. Landau, AIP Conf. Proc. **10**, 1163 (1973).

[10] D. E. Wrege, S. Spooner, and H. A. Gersch, AIP Conf. Proc. **5**, 1334 (1971).

[11] A. Mattila, T. Pylkkänen, J.-P. Rueff, S. Huotari, G. Vankó, M. Hanfland, M. Lehtinen, and K. Hämäläinen, J. Phys.: Condens. Matter **19**, 386206 (2007).

[12] H. Shi, W. Luo, B. Johansson, and R. Ahuja, Phys. Rev. B **78**, 155119 (2008).

[13] B. Lavina, P. Dera, R. T. Downs, W. Yang, S. Sinogeikin, Y. Meng, G. Shen, and D. Schiferl, Phys. Rev. B **82**, 064110 (2010).

[14] V. Cerantola, C. McCammon, I. Kupenko, I. Kantor, C. Marini, M. Wilke, L. Ismailova, N. Solopova, A. Chumakov, S. Pascarelli, and L. Dubrovinsky, Am. Mineral. **100**, 2670 (2015).

[15] B. M. French, Am. J. Sci. **271**, 37 (1971).

[16] V. P. Glazkov and I. N. Goncharenko, Fizika I Technika Vysokih Davlenij **1**, 56 (1991) (in Russian).

[17] J. Rodríguez-Carvajal, Physica B **192**, 55 (1993).

[18] P. E. Blöchl, Phys. Rev. B **50**, 17953 (1994).

[19] G. Kresse and J. Furthmüller, Comput. Mater. Sci. **6**, 15 (1996); Phys. Rev. B **54**, 11169 (1996).

[20] G. Kresse and D. Joubert, Phys. Rev. B **59**, 1758 (1999).

[21] H. J. Monkhorst and J. D. Pack, Phys. Rev. B **13**, 5188 (1976).

[22] P. E. Blöchl, O. Jepsen, and O. K. Andersen, Phys. Rev. B **49**, 16223 (1994).

[23] B. L. Gyorffy, A. J. Pindor, J. Staunton, G. M. Stocks, and H. Winter, J. Phys. F: Met. Phys. **15**, 1337 (1985).

[24] A. V. Ponomareva, Yu. N. Gornostyrev, and I. A. Abrikosov, Phys. Rev. B **90**, 014439 (2014).

[25] B. Alling, T. Marten, and I. A. Abrikosov, Phys. Rev. B **82**, 184430 (2010).

[26] A. I. Liechtenstein, M. I. Katsnelson, and V. A. Gubanov, Solid State Commun. **54**, 327 (1985).

[27] J. P. Perdew, K. Burke, and M. Ernzerhof, Phys. Rev. Lett. **77**, 3865 (1996).

[28] S. L. Dudarev, G. A. Botton, S. Y. Savrasov, C. J. Humphreys, and A. P. Sutton, Phys. Rev. B **57**, 1505 (1998).

[29] S. Lobanov, A. Goncharov, and K. Litasov, Am. Mineral. **100**, 1059 (2015).

[30] F. J. Birch, J. Geophys. Res. **91**, 4949 (1986).

[31] J. Zhang and R. J. Reeder, Am. Mineral. **84**, 861 (1999).

[32] J. B. Goodenough, *Magnetism and the Chemical Bond* (Interscience, New York, 1963).

[33] D. Bloch, J. Phys. Chem. Solids **27**, 881 (1966).

[34] G. Farfan, S. Wang, H. Ma, R. Caracas, and W. L. Mao, Am. Mineral. **97**, 1421 (2012).

[35] L. Chai and A. Navrotsky, Am. Mineral. **81**, 1141 (1996)

[36] X. Ming, X.-L. Wang, F. Du, J.-W. Yin, C.-Z. Wang, and G. Chen, J. Alloys Compd. **510**, L1 (2012).

[37] V. Badaut, P. Zeller, B. Dorado, and M. L. Schlegel, Phys. Rev. B **82**, 205121 (2010).

[38] D. M. Sherman, Am. Mineral. **94**, 166 (2009).

[39] R. F. W. Bader, *Atoms in Molecules: A Quantum Theory* (Clarendon Press, Oxford, 1994).

[40] B. Silvi and A. Savin, Nature **371**, 683 (1994).